PAPER

Study of low-velocity impact response of sandwich panels with shear-thickening gel cores

IOP Publishing Smart Materials and Structures
Smart Mater. Struct. 27 (2018) 065008 (14pp) https://doi.org/10.1088/1361-665X/aab7dc

Study of low-velocity impact response of sandwich panels with shear-thickening gel cores

Yunpeng Wang, Xinglong Gong[1] and Shouhu Xuan[1]

CAS Key Laboratory of Mechanical Behavior and Design of Materials, Department of Modern Mechanics, University of Science and Technology of China (USTC), Hefei 230027, People's Republic of China

E-mail: gongxl@ustc.edu.cn and xuansh@ustc.edu.cn

Received 17 January 2018, revised 8 March 2018
Accepted for publication 19 March 2018
Published 3 May 2018

Abstract

The low-velocity impact response of sandwich panels with shear-thickening gel cores was studied. The impact tests indicated that the sandwich panels with shear-thickening gel cores showed excellent properties of energy dissipation and stress distribution. In comparison to the similar sandwich panels with chloroprene rubber cores and ethylene-propylene-diene monomer cores, the shear-thickening gel cores led to the obviously smaller contact forces and the larger energy absorptions. Numerical modelling with finite element analysis was used to investigate the stress distribution of the sandwich panels with shear-thickening gel cores and the results agreed well with the experimental results. Because of the unique mechanical property of the shear-thickening gel, the concentrated stress on the front facesheets were distributed to larger areas on the back facesheets and the peak stresses were reduced greatly.

Keywords: low-velocity impact, sandwich panels, shear-thickening gel, numerical simulation

(Some figures may appear in colour only in the online journal)

1. Introduction

Sandwich structure usually composes of thin high-strength facesheets or skins and thick light-density functional cores. Due to its relatively light weight and efficient in supporting transverse loads, sandwich structure composite is one of the most popular materials used in engineering applications such as transportation, aerospace and aircraft industries, marine industries, wind turbine industries and so on [1–4]. It is well known that most of the bending forces in sandwich structure composites are supported by the facesheets while the shear loads are transferred by the core [2, 5, 6]. The mechanical properties of the core materials have significant influence on the performance of the sandwich panels [7, 8]. Various cores have been used to promote the performance of sandwich structure panels, such as honeycomb cores [9–11], balsa wood cores [7], foam cores [12–14], polyethylene cores [15], etc. In comparison with traditional core materials, smart materials have caught increasing attention [16–22]. Tanju Yildirim conducted experimental nonlinear dynamics of a sandwich beam with magneto-rheological elastomer core, and found the hardness of the beam was enhanced by the magnetic field [23, 24]. Shear thickening fluid has also been used as cores of sandwich structures to promote the vibration absorption, taking the advantage of its rate dependent mechanical properties [25, 26]. However, the lack of excellent impact resistance, restorability and stability is the application limitation of most smart materials used as sandwich cores at present.

Shear-thickening gel (STG) is a smart material with sensitive response to the impact loading [27–31]. In normal situation, STG is soft and viscous with great restorability. When applied external excitation of shear, compression, and tension, STG becomes stiff with its elastic modulus increasing sharply [32, 33]. As soon as the mechanical loading is removed, STG returns back to the initial viscous state. STG is a lightly cross-linked silicone polymer with reversible interactions of boron–oxygen (B–O) bonds [34]. Under low-rate mechanical stimuli, the entangled molecular chains were stretched and the B–O bonds were broken. The time was long

[1] Authors to whom any correspondence should be addressed.

enough for the disentanglement of the molecular chains. Under high-rate stimuli, the action time was short and the entangled molecular chains were locked, showing as the sharp increment of the elastic modulus in the macroscopic [33, 35]. In the whole progress of loading and unloading, the STG could absorb a lot of energy through the microfragmentation and disentanglement of the high weight molecular chains [33]. Due to the excellent performance of energy absorption and impact resistance, STG exhibited great potential in application as sandwich structure core materials. Different from the STF suspension with the sedimentation problem, STG was more stable. As sandwich cores, STG can not only show excellent impact energy absorption ability, but also have advantages of restorability and stability [36].

To investigated the impact response of sandwich panels, many works have been reported with impact tests from low velocity, medium velocity to high velocity [10, 17, 37–40]. Low-velocity impact tests with velocities less than 10 m s^{-1}, similar to some engineering application situations, were usually used to study the impact resistance properties of sandwich panels. However, most of the low-velocity impact tests were carried out with cylinder tube supports or square tube supports. The edges of sandwich panels were clamped and the central areas were not supported. When the objects to be protected did not contact the sandwich panels, the work conditions of the sandwich panels were similar to the cylinder supports. Nonetheless, in some situations, sandwich panels were used by wrapping or contacting the objects directly, of which the conditions were similar to the plate supports. Thus, impact tests with plate supports offering fixed boundary to back facesheets of sandwich panels are as necessary as that with cylinder supports.

In this work, low-velocity impact responses of sandwich structures with two different facesheets and three different cores were studied. A cylinder support and a plate support were used to offer two different experiment conditions to match different application situations. The energy absorption and the impact resistance of sandwich panels with STG cores, chloroprene rubber (CR) cores and ethylene-propylene-diene monomer (EPDM) cores were investigated and compared. Besides, the finite element analysis numerical simulations were carried out to compare with experimental results and investigate the stress distribution of the sandwich panels with STG cores.

2. Experiment

2.1. Materials and preparation

The STG was fabricated with boric acid (10043-35-3), dimethyl siloxane (9016-00-6), ethyl alcohol (64-17-5) and benzoyl peroxide (BPO, 94-36-0) (from Sinopharm Chemical Reagent Co. Ltd, Shanghai, China). The boric acid, dimethyl siloxane and ethyl alcohol are raw materials to prepare polymer matrix, and the BPO is the vulcanizing agent in the preparation. The preparing procedures of STG are as follows.

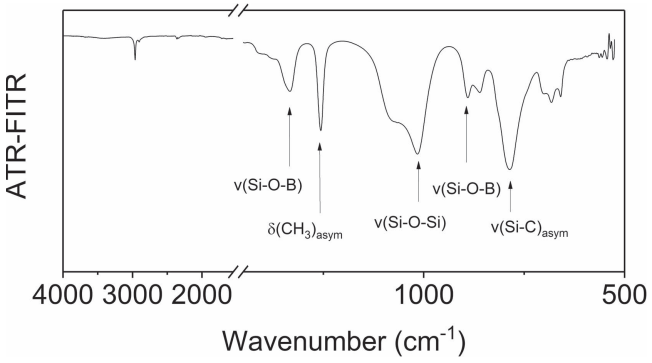

Figure 1. ATR-FITR spectroscopic characterization.

Firstly, boric acid was heated at 160 °C for 2 h to gain pyroboric acid. Secondly, 11 wt% pyroboric acid, 83 wt% dimethyl siloxane, and 6 wt% ethyl alcohol were mixed together and stirred well in a beaker. Then the mixture was heated at 240 °C for 7 h. When the mixture was cooled down to room temperature, it was put in a double-roll mill (Taihu Rubber Machinery Inc., China, model XK-160) and homogeneously mixed with BPO (at 40 mg/g. Then the new mixture was vulcanized at about 100 °C for 2 h. The final cooled product was STG. After cooling it to the room temperature, STG was obtained.

To investigate the chemical nature of STG, the ATR-FITR spectroscopy was done (figure 1). The IR spectra of STG are dominated by the characteristic stretching vibrations of Si–C (790 cm^{-1}), Si–O–Si (1015 and 1075 cm^{-1}) along with the asymmetric deformation mode of $–CH_3$ at 1260 cm^{-1}. The vibration at 870 and 1340 cm^{-1}, which can be assigned to the Si–O–B stretching vibration demonstrating successful cross linking of the PDMS with the boric acid. The breaking and reformations of B–O bonds could absorb lots of energy, which has been investigated in our previous woks [33, 35]. The Si–O–Si bonds constituted the molecules of STG instead of the common C–C bonds.

Taking STG, CR and EPDM plates as cores, and aluminium plates and chloroprene rubber plates as facesheets, six different sandwich panels were manufactured and their masses were listed in the table 1 (e.g. Al-STG-Al sandwich has Al facesheets and STG core). The sandwich panels composed of 2 mm thick facesheets and 8 mm thick cores, and all the sandwich panels were 250 mm × 250 mm × 12 mm. The density and the Young's modulus of the aluminium (Al) 5052-H18 (from Hongwang Mould Limited, Shenzhen, China) were refer to previous reports [41, 42], and the density and the Young's modulus of CR (from Shanghai Jingxiang Industrial Limited, Shanghai, China) and EPDM (from Shanghai Juxiong Limited, Shanghai, China) were obtained from the manufacturers, listed in table 2. The Young's modulus of STG was dependent on the mechanical loading. The STG core was a cylinder with a diameter of 200 mm and a thickness of 8 mm. The facesheets were adhered to the STG cores. A 22.5 mm wide strip rectangle block made of polyethylene was used to separate the facesheets to control the thickness of the STG cores (figures 2(b) and (d)). The CR cores and EPDM cores were glued to the Al facesheets and

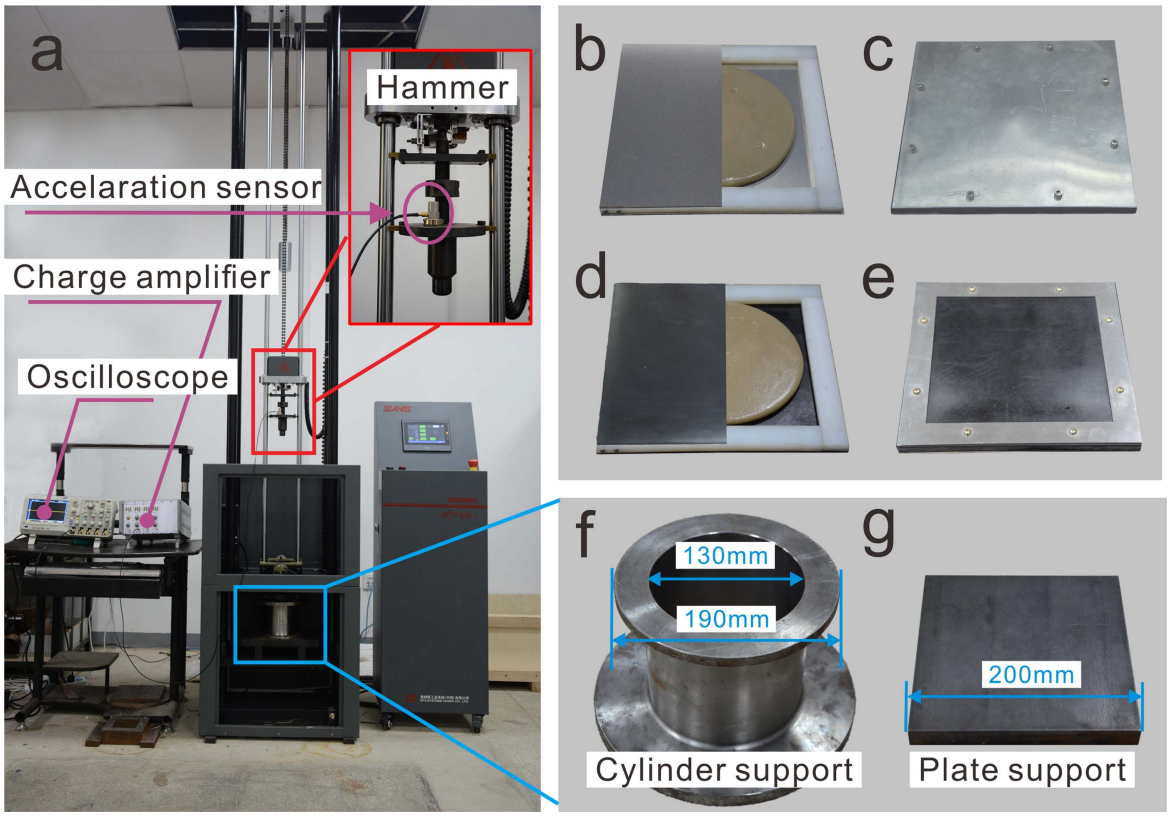

Figure 2. (a) The drop-testing machine and the data acquisition system; different sandwich panels: (b) Al-STG-Al sandwich, (c) Al-EPDM-Al sandwich and Al-CR-Al sandwich, (d) CR-STG-CR sandwich and CR-EPDM-CR sandwich, (e) pure CR; (f) cylinder support; (g) plate support.

Table 1. The masses of different sandwich panels.

Sandwich panels	Al-STG-Al	Al-CR-Al	Al-EPDM-Al	CR-STG-CR	CR-EPDM-CR	Pure CR
Total mass/kg	0.96	1.45	1.54	0.67	1.22	1.13

Table 2. The density and the Young's modulus of the materials.

Materials	Al 5052-H18	CR	EPDM	STG
Density	2785 kg m^{-3}	1540 kg m^{-3}	1710 kg m^{-3}	1010 kg m^{-3}
Young's modulus	71 GPa	13.4 MPa	9.74 MPa	—

CR facesheets and reinforced through bolted connections. Two 22.5 mm wide strip rectangle blocks made of stainless steel were bolted connected to clamp the edges of CR-EPDM-CR sandwich and Pure CR plate to keep them flat (figures 1(c), (e)).

2.2. Impact testing

The impact performance of the sandwich panels was investigated by a drop-testing machine (Mode ZCJ1302-A, MTS Industrial Systems (China) CO., LTD, China) (figure 2(a)). The hammer was 2 kg weight and its impact head was 25 mm in diameter (D25 standard hammer). A charge amplifier (Mode YE5853, Jiangsu Sinocera Piezotronics. INC., China) and an oscilloscope (Mode DPO2012B, Tektronix INC., USA) with a sampling rate of 100 kHz were employed to analyse experimental data collected by a piezoelectric acceleration sensor. The cylinder support, made of mild steel, had a 130 mm inner diameter and a 190 mm outer diameter (figure 2(f)). The plate support was a 200 mm × 200 mm flat square plate made of structure steel (figure 2(g)). In the impact tests, the sandwich panels were settled on the centre of the supports. The hammer free fell from the height of 50, 100 and 200 cm and impacted the sandwich panels perpendicularly. The friction between the hammer and the guide rails was neglected. The impact velocities of the hammer were calculated with following equations:

$$v_0 = \sqrt{2gh}, \tag{1}$$

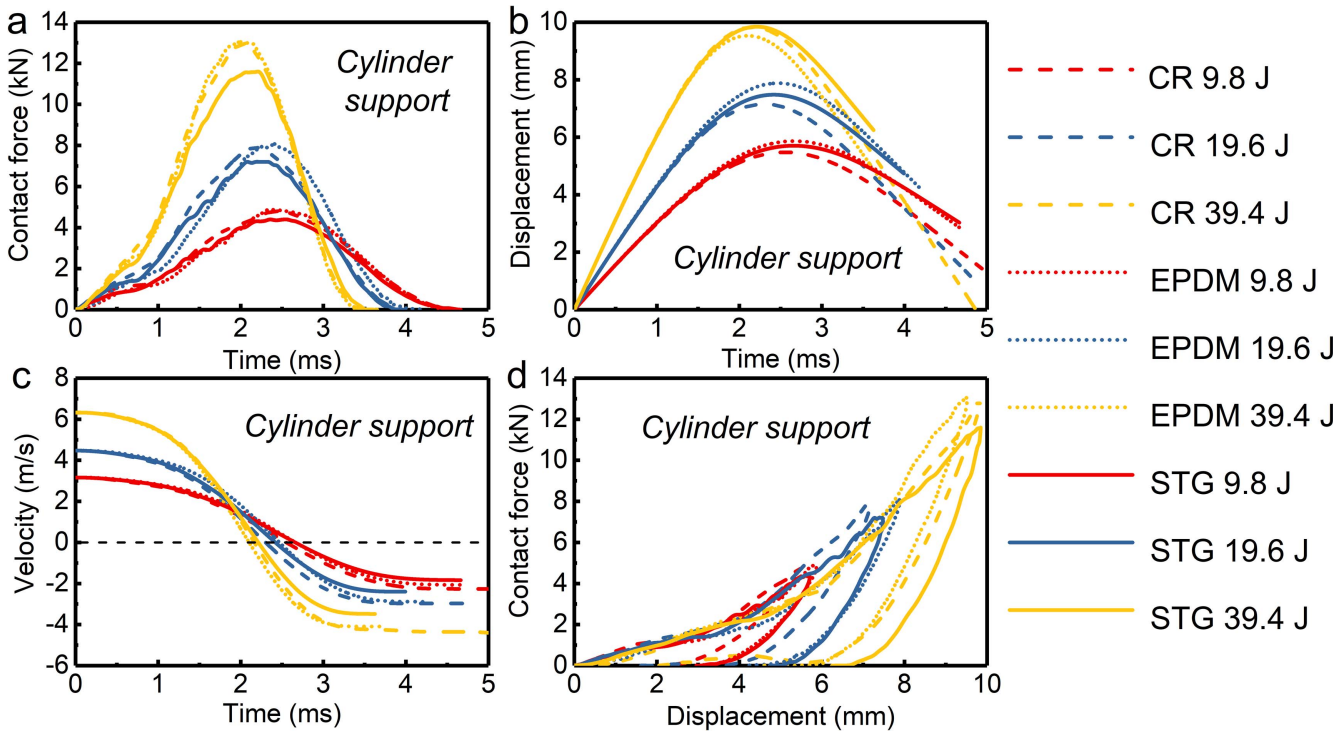

Figure 3. Impact response of Al facesheets sandwich panels with different cores in the impact tests with cylinder support. (a) Contact forces between the hammer and the sandwich panels, (b) displacements of the hammer, (c) velocities of the hammer, and (d) contact force–displacement curves.

$$v(t) = v_0 + \int_0^t a(\tau)\mathrm{d}\tau, \tag{2}$$

where v_0 is the impact velocity while the hammer reaching to the front facesheets of the panels, g is standard gravity, h is falling height of the hammer, $v(t)$ is velocity of the hammer along with time variation in the impact progress, and $a(t)$ is acceleration of the hammer varying with time. The displacements of the hammer while it contacted the front facesheet were calculated with the equation as follows:

$$x(t) = \int_0^t v(\tau)\mathrm{d}\tau, \tag{3}$$

where $x(t)$ is the downwards vertical displacement of the hammer while it contacted the front facesheets of the panels. With different falling heights, the impact energies could be calculated with equation (3).

$$E_0 = mgh, \tag{4}$$

where E_0 is the impact energy and m is the mass of the hammer, i.e., 2 kg. Thus, the impact energies are 9.8 J, 19.6 J and 39.4 J, respectively.

3. Results and discussion

3.1. Impact tests with cylinder support

The Al facesheets sandwich panels with different cores were firstly impacted with cylinder support. With the data acquisition system and the calculation through equations (2) and (3), the curves of contact forces, displacements, velocities and contact force–displacement were obtained, shown in figure 3.

The contact force curves showed similar tendency along the time (figure 3(a)). The start sections of all the curves were relatively flat, because the front facesheet provided the main acting force under impact. With the deformation of the front facesheet, the core and the back facesheet started to resistant the impact, causing the curves increasing sharply. When the velocities of the hammer decreased to 0, the contact forces and the displacements reached to the peak values simultaneously. In the impact tests with higher impact energy, the contact forces of sandwich panels with all kinds of cores were larger. Impacted with the same impact energy, the STG core sandwich afforded lower contact force than the CR core sandwich and EPDM core sandwich. It demonstrated that STG cores had better impact resistance than CR cores and EPDM cores.

When the impact energy increased from 9.8 J to 19.6 J to 39.4 J, the contact forces, the displacements and the initial velocities increased proportionally (figures 3(a)–(c)). In the tests with the same impact energy, the displacements of sandwich panels with CR cores, EPDM cores and STG cores were similar to each other, which means the Al facesheets had similar deformations and the core materials caused the main differences in the impact resistance. After the hammer reached to the lowest points, it rebounded in an opposite direction till the hammer and the sandwich panels separated. When they separated, the main remanent mechanical energy was the kinetic energy of the hammer. The final velocities in the 19.6 J impact tests of sandwich panels with CR cores,

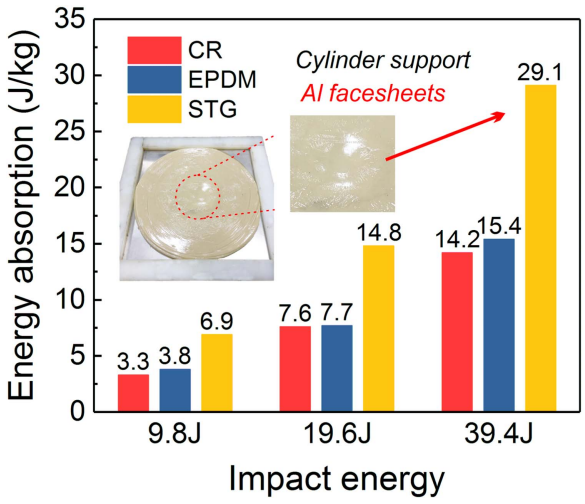

Figure 4. Energy absorption of Al facesheets sandwich panels with different cores in the impact tests with cylinder support. Insert is the picture of STG core after the impact with 39.6 J energy.

EPDM cores and STG cores were $-2.97\ \mathrm{m\,s^{-1}}$, $-2.89\ \mathrm{m\,s^{-1}}$ and $-2.40\ \mathrm{m\,s^{-1}}$ respectively (negative signs mean the velocities were in the opposite directions to the initial velocities). The lower absolute values of final velocities proved that the STG core sandwich panels absorbed more impact energy than the CR core and EPDM core sandwich panels.

To investigate the energy absorptions in the impact tests, the contact force–displacement curves were plotted through combining the contact force curves and the displacement curves (figure 3(d)). The contact forces increased with the increasing displacements at beginning and decreased after reaching to the peak values. The area enveloped by the curve and x axis was the work done by the sandwich panel, and it was deemed as the absorbed energy in the impact tests [7]. With different impact energy, the STG core sandwich panels absorbed about 75% of the impact energies, while the CR core and EPDM core panels absorbed about 53% and 57% energies, respectively. The energy absorptivity was calculated by dividing the absorbed energy by the impact energy.

The specific energy absorption of unit mass was shown in figure 4. With different impact energy, the energy absorption of sandwich panels with STG cores was obviously larger than that of sandwich panels with CR cores or EPDM cores. When the impact energy increased, the energy absorption of sandwich panels increased proportionally.

3.2. Impact tests with plate support

3.2.1. Aluminium facesheets sandwiches. The impact response of the Al facesheets sandwich panels was also investigated with plate support. With three different impact energy, 9.8 J, 19.6 J and 39.4 J, the curves of contact forces, displacements, velocities and contact force–displacement were shown in figure 5.

The contact force curves of sandwich panels with STG cores was relatively flat compared with those of sandwich panels with CR cores and EPDM cores in the impact tests with the same impact energy (figure 5(a)). Similarly, in the impact tests with the same impact energy, the STG core sandwich afforded obviously lower contact force than the CR core sandwich and EPDM core sandwich. With lower contact force, STG core sandwich panels exhibited better impact buffering ability than CR core sandwich panels and EPDM sandwich panels. Comparing to the results in the tests with cylinder support, the contact force with plate support was larger. With the fixed boundary of the back facesheets, the deformation of sandwich panels was smaller and the action time was shorter in the tests with plate support, leading the panels to afford larger force to provide the similar impulse.

The displacements and the velocities of the hammer changed with the contact forces in the tests synchronously (figures 5(b) and (c)). When the contact force reached to the peak value, the velocity decreased to 0 and the hammer reached to the lowest position with the largest displacement. The maximum displacements in the tests with STG core sandwich panels were larger than those in the tests with CR core sandwich panels and EPDM sandwich panels, while their final velocities were similar. Under the impact with plate support, the STG below the impact hammer was squeezed into the surrounding area (figure 6 insert). The squeezed flow of STG led the impact stress to be distributed into the whole area of the back facesheet. Thus, the deformation of STG panel was larger and the force was much smaller. According to the theorem of momentum, the different sandwich panels provided similar impulse to the hammer under the same impact energy. While the contact force was lower, the action time would be longer and the displacements would be larger.

To investigate the energy absorptions in the action progress, the contact force–displacement curves were plotted (figure 5(d)). The increasing slopes of the curves reflected the compression strength of the sandwich panels. The sandwich panels with STG cores had relatively lower strength than the sandwich panels with CR cores and EPDM cores. The areas enveloped by all the curves were the energy absorbed by the different sandwich panels. With different impact energy, the sandwich panels with CR cores, EPDM cores and STG cores absorbed about 79%, 84% and 82% energies, respectively.

The specific energy absorptions of unit mass were shown in figure 6. STG core sandwich panels absorbed obviously more energy per unit mass than CR core and EPDM core sandwich panels in the tests with the same impact energy. In the tests with both cylinder support and plate support, STG cores showed more excellent impact resistance and energy absorption than CR cores and EPDM cores.

3.2.2. Chloroprene rubber facesheets sandwiches. Flexible sandwich panels with CR facesheets were also investigated in the impact tests with plate support. The CR facesheet panel was a flexible sandwich panel which was able to be applied to protect the objects by coating them. Thus, the working situation of CR facesheet panel was similar to the plate support. The experimental results were shown in figure 7. With the same impact energy, the contact force of CR-STG-CR sandwich panels was obviously smaller than that of pure CR plates and CR-EPDM-CR sandwich panels (figure 7(a)).

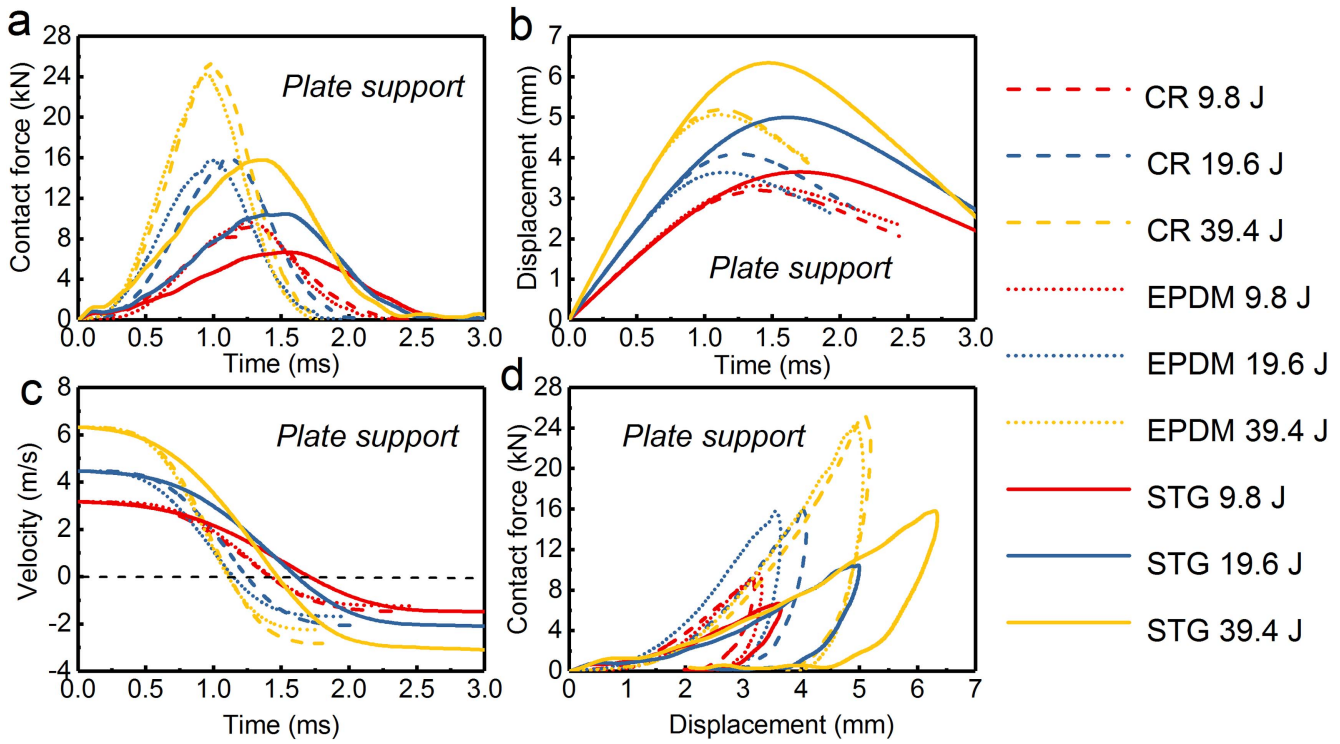

Figure 5. Impact response of Al facesheets sandwich panels with different cores in the impact tests with plate support. (a) Contact forces, (b) displacements, (c) velocities, and (d) contact force–displacement curves.

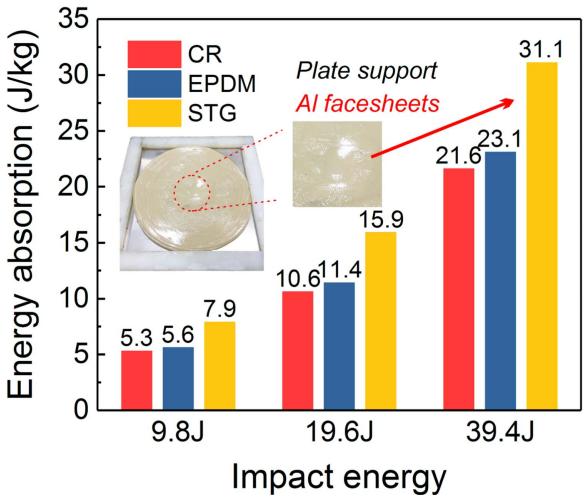

Figure 6. Energy absorption of Al facesheets sandwich panels with different cores in the impact tests with plate support. Insert is the picture of STG core after the impact with 39.6 J energy.

It was noticed that the contact force curve of sandwich panels with STG cores in the test with 39.4 J impact energy had a relative extremum before the maximum value. Under the high energy strike, STG transformed into rubbery state to provide the supporting force at first. When the CR front facesheet suffering large deformation, the yielded STG was broken and was further squeezed to the surrounding area, showing as the first drop of the contact force (figure 8 insert). Then, the two CR facesheets contacted and provided the main supporting force, causing the second rise of the contact force. The elastic modulus of CR was much larger than STG, which was the reason for the sharp drop of the last section of the curve. The fracture and movement of STG in the whole progress absorbed a large amount of impact energy and distributed the stress to the whole panel. Comparing with the CR facesheets, Al facesheets had much larger modulus and suffered smaller deformation. Thus, there was not the second relative extremum in the contact force curve of Al facesheets sandwich panels.

With much longer action time, the displacements in the tests of STG core sandwich panels were larger than those of EPDM core sandwich panels and pure CR panels (figure 7(b)). When the displacements increased to the maximum values, the velocities decreased to 0. With the same impact energy, the final velocities in the tests of CR-STG-CR sandwich panels were much lower than the velocities in the tests of pure CR panels and CR-EPDM-CR sandwich panels (figure 7(c)). With lower final velocity, the sandwich panels with STG cores absorbed much more impact energy in the tests.

Combining the contact force curves and the displacement curves, the relationship between the contact force and the displacement was studied, as shown in figure 7(d). Having flatter increasing slopes, the curves of STG core sandwich panels reflected the compression strength was lower than the pure CR panels and EPDM core panels. The energy absorbed by the sandwich panels in the impact tests was represented as the areas enveloped by the contact force–displacement curves and x-axis. The energy absorptions of unit mass were shown in figure 8. With the same drop height, the CR-STG-CR sandwich panels absorbed much more energy per unit mass than the pure CR panels and the CR-EPDM-CR sandwich

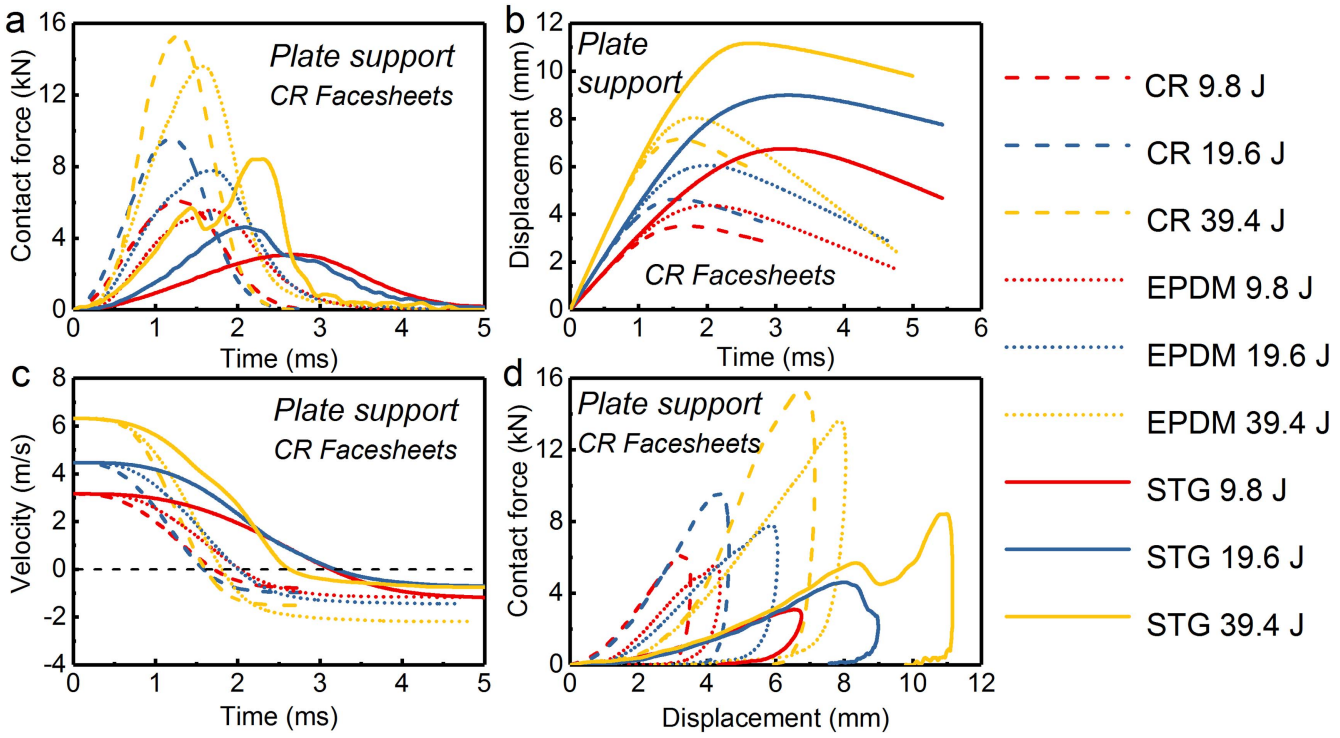

Figure 7. Impact response of CR facesheets sandwich panels with different cores in the impact tests with plate support. (a) Contact forces, (b) displacements, (c) velocities, and (d) contact force–displacement curves.

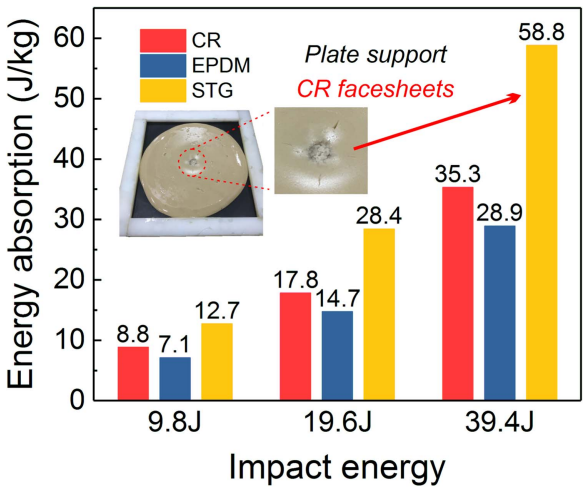

Figure 8. Energy absorption of CR facesheets sandwich panels with different cores in the impact tests with plate support. Insert is the picture of STG core after the impact with 39.6 J energy.

panels. Based on above results, the sandwich panels with STG cores were demonstrated to have excellent capacities of impact resistance and energy absorption.

Comparing the impact response of sandwich panels with Al facesheets and CR facesheets, the contact force of CR facesheets sandwich panels was smaller while the energy absorption was larger. Flexible sandwich panels with STG cores showed excellent impact resistance and energy absorption. With the same facesheets, STG core sandwich panels had the best performance in reducing the contact force and absorbing the impact energy. It could be concluded that the sandwich panels with STG cores had greater potential in the application of impact resistance and protection than the sandwich panels with CR cores and EPDM cores.

In natural state, STG shows viscous-flow characters with low elastic modulus. Under low-rate mechanical stimuli, the entangled molecular chains are stretched and disentangled. The reversible interactions of B–O bonds provide the main force and some of the bonds are broken and reformed [34]. When the strain rate increases, the entangled molecular chains are difficult to disentangle. More B–O bonds take action causing the increase of the modulus. With high-rate mechanical stimuli, the action time is short and the entangled molecular chains are locked. The molecular chains play the main role and the elastic modulus becomes a lot larger in the macroscopic [33, 43].

As cores in the sandwich structures, STG transformed from viscous-flow state to rubbery state and the glassy state immediately under the hammer's impact [32, 33]. With the deformation of the front facesheet, the STG yielded. The STG in the central area was broken and squeezed to the surrounding areas. During the fracture and the movement of the STG, the impact energy was dissipated and the force was distributed to the whole sandwich panel. Different from STG, CR and EPDM cores were in the elastomeric state all the way. The CR and EPDM cores were compressed with the deformation of the front facesheets. Most of the impact energy was reserved in the material as the strain energy. When the hammer bounced back, the reserved energy was released. Thus, the energy dissipation and the force distribution of STG were much better than CR and EPDM. In addition, STG returned back to the initial viscous-flow state

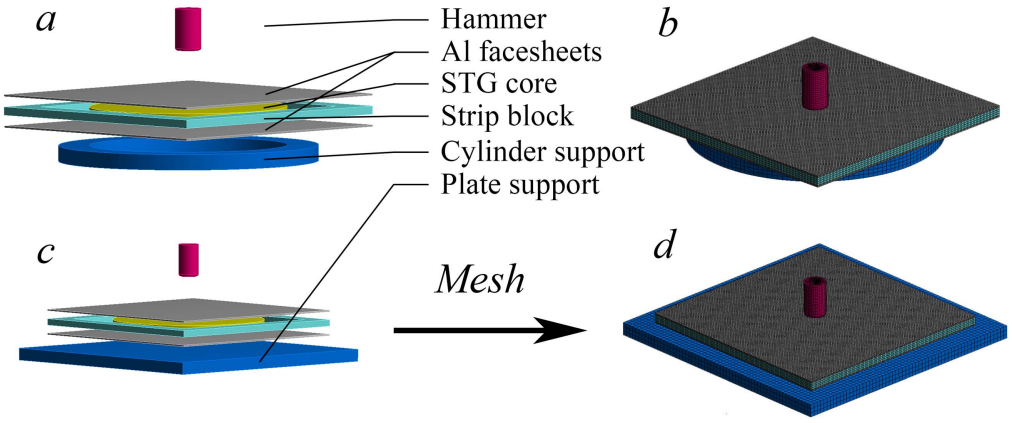

Figure 9. Finite element model for the impact tests with cylinder support (a), (b) and plate support (c), (d).

as soon as the impact was unloaded. The restorability of STG could broaden the potential application in impact resistance and cushioning protection.

4. Numerical simulation

4.1. Finite elements analysis simulation

In the impact tests, the stress distributions on the front facesheets and the back facesheets were not able to be obtained. Thus, the finite elements analysis (FEA) simulations of Al-STG-Al sandwich panels were carried out to investigate the stress distribution. ANSYS Workbench 16.0 was chosen for the simulation.

Impact tests with both plate support and cylinder support were modelled. The geometry was modelled referring to practical sizes of the sandwich panels, the hammer and the supports (figure 9). The STG core was a cylinder with a diameter of 200 mm and a thickness of 8 mm. The sandwich panels were 250 mm × 250 mm × 12 mm in size with 2 mm thick Al facesheets. The hammer was simplified as a cylinder with 40 mm in height and 25 mm in diameter. The circle edge of the hammer head was rounded with a radius of 3 mm. The thickness of supports was set as 15 mm.

The mechanical properties of Al 5052-H18 are as follows, density $\rho = 2680\,\mathrm{kg\,m^{-3}}$, Young's module $E = 69.3$ Gpa, Poisson ratio $\upsilon = 0.33$, yield stress $\sigma_0 = 215$ Mpa. The Cowper–Symonds model, as a common rate-dependent constitutive model, was chosen for Al 5052-H18 facesheets and STG cores. In Cowper–Symonds model, the dynamic yield stress is dependent on the strain rate with the relation $\mathrm{d}\varepsilon/\mathrm{d}t = C(\sigma_y/\sigma_0 - 1)^q$, where σ_0 is static yield stress, $\mathrm{d}\varepsilon$ is the strain increment in time increment $\mathrm{d}t$, and σ_y is dynamic yield stress, constants C and q can be identified by particular experiments. For Al 5052-H18, the constant $C = 1.7 \times 10^6$ and $q = 4$ [41]. The mechanical properties of STG were obtained from experiments. The density $\rho = 1010\,\mathrm{kg\,m^{-3}}$, and the Poisson's ratio ν is taken as 0.5. According to the quasi-static steady shear results (figure 10(b)), the elastic modulus E is 60 Pa using the $E = 2G(1 + \nu)$, where G is shear modulus.

According to Cowper–Symonds model, the relationship of yield stress σ_Y and effective plastic strain $\varepsilon_p^{\mathrm{eff}}$ and strain rate $\dot{\varepsilon}$ can be expressed as the following equation [44, 45]:

$$\sigma_Y = \left[1 + \left(\frac{\dot{\varepsilon}}{C}\right)^{\frac{1}{q}}\right][A + B(\varepsilon_p^{\mathrm{eff}})^n], \tag{5}$$

where A is the initial yield stress, B is the plastic hardening parameter, n is the plastic strain index, C and q are the rate dependent parameters. Due to the relaxation of STG, the shear tests data is more convenient to gain than the compressive tests data. In shear, the equation S.1 could be replaced as follows

$$\tau_Y = \left[1 + \left(\frac{\dot{\gamma}}{C}\right)^{\frac{1}{q}}\right][A + B(\gamma_p^{\mathrm{eff}})^n], \tag{6}$$

where τ_Y is the yield shear stress, γ_p^{eff} is the effective plastic shear strain, and $\dot{\gamma}$ is shear rate. In quasi-static shear, the equation will be simplified as

$$\tau_Y = A + B\gamma^n. \tag{7}$$

The rheology properties of STG were tested by a rheometer (Physica MCR 302, Anton Paar Co., Austria). The STG specimens were kept at 1 mm thick and tested with PP20/MRD/TI parallel plate geometry. The angular frequency oscillatory shear tests were carried out with a strain of 0.1% at the temperature of 25 °C (figure 10(a)). The storage modulus increased about five orders of magnitude with the increasing of angular frequency. The loss modulus increased with the storage modulus at first and decreased after reaching its peak values, where the loss modulus and the storage modulus were equal. The oscillatory shear result showed the excellent shear-thickening performance of STG. The steady shear test at the shear rate of 0.001 $\mathrm{s^{-1}}$ was also carried out by the rheometer (figure 10(b)).

Fitting the quasi-static shear stress-strain curve with equation (7), the parameters A, B and n were obtained (figure 11). And it was obvious that the Cowper–Symonds model could well describe the quasi-static shear test result.

Thus, the equation (6) was expressed as

$$\tau_Y = \left[1 + \left(\frac{\dot{\gamma}}{C}\right)^{\frac{1}{q}}\right][14.88 + 7.256(\gamma_p^{\mathrm{eff}})^{0.622}]. \tag{8}$$

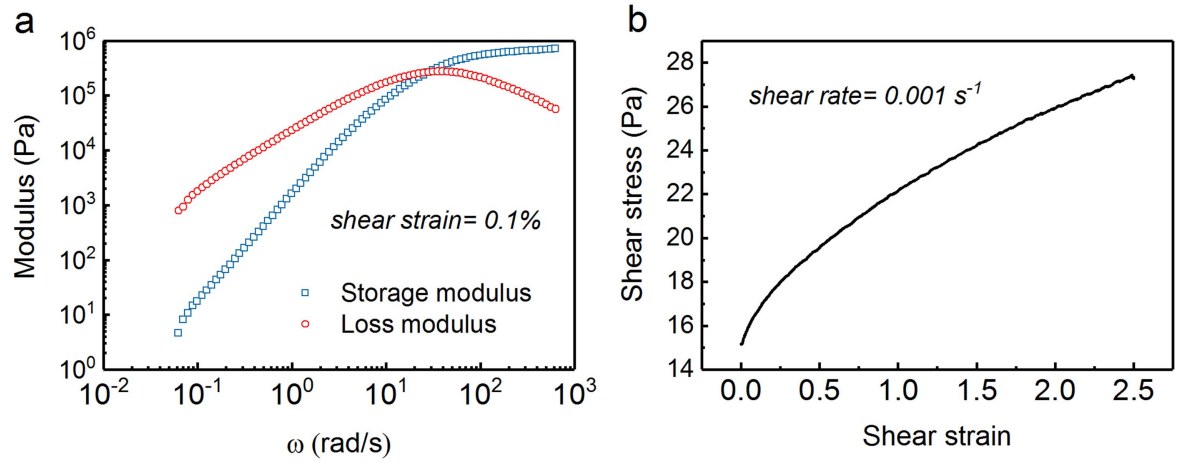

Figure 10. (a) Oscillatory shear test and (b) quasi-static steady shear test of STG.

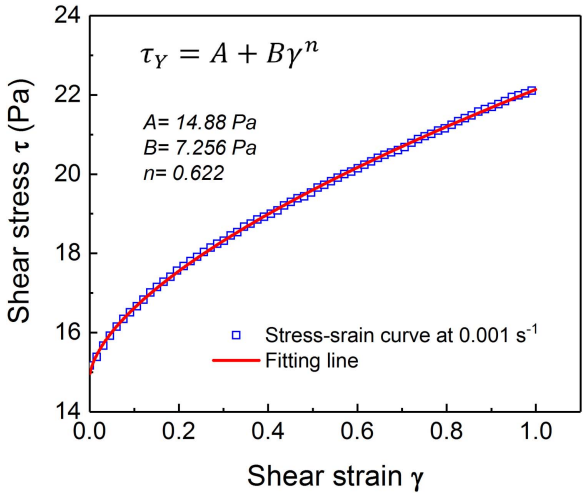

Figure 11. Quasi-static shear curve of STG and the fitting line with Cowper–Symonds model.

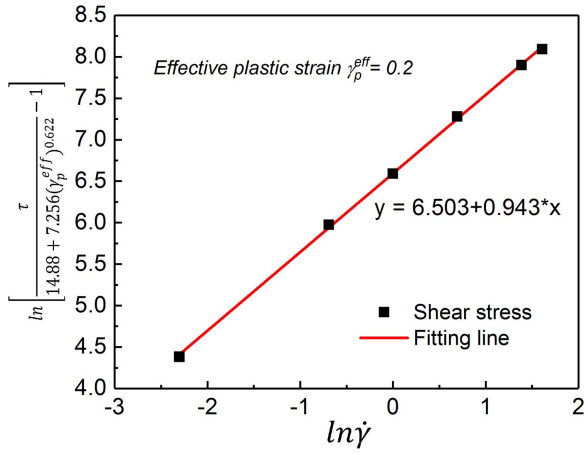

Figure 12. Linear fitting of the shear stress at the effective strain of 0.2 with different shear rate.

Taking the logarithm of both sides, it was transformed into

$$\ln\left[\frac{\tau}{14.88 + 7.256(\gamma_p^{\text{eff}})^{0.622}} - 1\right] = \frac{1}{q}\ln\dot{\gamma} - \frac{1}{q}\ln C. \quad (9)$$

The shear stress–strain curves of STG were obtained though steady shear tests with different shear rate (0.1, 0.5, 1.0, 2.0, 4.0 and 5.0 s^{-1}). The linear fitting with equation (9) of the shear stress at the effective strain of 0.2 with different shear rate was shown in figure 12. The slope of the fitting line is $1/q$ and the intercept is $-\ln C/q$. According to the fitting line, it could be calculated that $q = 1.06$ and $C = 1.012 \times 10^{-3}\ s^{-1}$.

The final constitutive equation of STG referring to Cowper–Symonds model was obtained as follows:

$$\tau_Y = \left[1 + \left(\frac{\dot{\gamma}}{1.012 \times 10{-}3}\right)^{\frac{1}{1.06}}\right][14.88 + 7.256 \times (\gamma_p^{\text{eff}})^{0.622}]. \quad (10)$$

According to equation (10), the shear stress–strain curves were plotted in figure 13 and were compared with the steady shear results. With different shear rate, the Cowper–Symonds model results fitted the experimental curves well.

The shear constitutive equation (10) could be converted to compressive constitutive equation through $E = 2G(1 + \nu)$ where ν was Poisson's ratio which was taken as 0.5 for STG [29]. The final constitutive equation for STG was as follows.

$$\sigma_Y = \left[1 + \left(\frac{\dot{\varepsilon}}{1.012\times10{-}3}\right)^{\frac{1}{1.06}}\right][44.64 + 21.795 \times (\varepsilon_p^{\text{eff}})^{0.622}]. \quad (11)$$

The hammer was modelled with structural steel model in engineering data and its density was adjusted to $1.022 \times 10^5\ kg\ m^{-3}$ to fit the practical mass. Both the plate support and the cylinder support were modelled using structural steel model. The material model of the polyethylene strip rectangle blocks was available in engineering data. All the objects were set as solid elements. The stiffness behaviours of the hammer and the supports were set as rigid, and the rest objects were flexible.

Table 3. The nodes and elements of the objects.

	Front facesheet	Back facesheet	Hammer	Cylinder support	Plate support	Strip blocks	STG core
Nodes	47628	47628	7659	4680	51984	31385	61146
Elements	31250	31250	6908	3436	45000	23312	50280

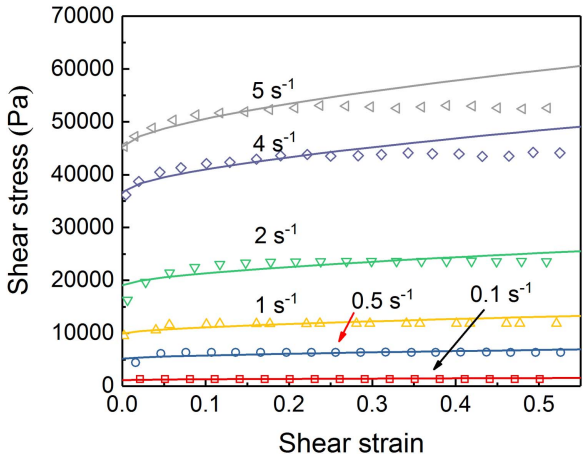

Figure 13. Shear stress–strain curves of STG. The solid lines are Cowper–Symonds model fitting results and the scatterplots are steady shear results testing with the rheometer.

The geometry was meshed with an element size of 2 mm, and the thickness dimension edges of the sandwich panels was meshed with an edge element size of 1 mm, and the supports were meshed with a body element size of 5 mm. After meshing with explicit shape checking, the nodes and elements of all the objects were listed in table 3. The average element quality was 0.877.

The body interactions between the facesheets and the STG core, the facesheets and the polyethylene strip rectangle blocks were bonded. The body interactions between the hammer and the front facesheet, the back facesheet and the support were frictional with a friction coefficient of 0.3 (the friction coefficient between the aluminium plate and the structure steel plate is generally considered to be 0.3). The velocities of 3162, 4472 and 6324 mm s^{-1} were applied to the hammer as the initial conditions. Fixed supports was applied to the plate support and the cylinder support. Standard Earth gravity was applied with y direction, and only the y component of the hammer's displacement was set free.

4.2. Numerical simulation results

The contact forces in the simulation of impact tests with both cylinder support and plate support were compared with the experimental results. As shown in figure 14, the numerical and experimental agreed well. With both cylinder support and plate support, the experimental and numerical maximum forces were similar. The validity of numerical model is verified with the maximum contact force, listed in table 4. The error rate was calculated by

$$\text{Error rate} = \frac{|\,\text{Max Num.force} - \text{Max Exp.force}\,|}{\text{Max Exp.force}} \times 100\%. \quad (12)$$

The error rates of the numerical simulations were within 5%, demonstrating the validity of the numerical models. The stress distribution in the front and back facesheets in the FEA simulation was expressed with Von Mises equivalent stress which could reflect the distribution of the strain energy. The Von Mises equivalent stress is based on the fourth strength theory and is calculated by

$$\sigma_e = \sqrt{\frac{(\sigma_1-\sigma_2)^2+(\sigma_2-\sigma_3)^2+(\sigma_3-\sigma_1)^2}{2}}, \quad (13)$$

where σ_e is the Von Mises equivalent stress, and σ_1, σ_2, and σ_3 are the first, the second, and the third principal stress, respectively.

The equivalent stress distributions in the simulation with cylinder support was shown in figure 15. In the front facesheet, the stress was concentrated in the central area. In the back facesheet, the stress was distributed to a much larger area, and the maximum stress was a lot smaller than that in the front facesheet. Taking the simulation with 19.8 J impact energy for example, the maximum stress in the front facesheet and the back facesheet were 266 MPa and 41.7 MPa, respectively. When the impact transmitted from the front facesheet, through the STG core, to the back facesheet, the impact force was distributed to the whole panels and dissipated by the interaction, the friction, and the movement of the STG. When the impact energy increased, the stress in the facesheets increased correspondingly, but the stress distribution was shown in similar ways. By reducing the maximum stress and distributing the concentrated stress, the STG sandwich panels exhibited good impact resistance.

Analogously, the stress distribution in the front and back facesheets in the FEA simulation with plate support was shown in figure 16. Similarly, the stress in the front facesheets concentrated in the centre area, while the stress in the back facesheets was distributed to almost the whole area. The maximum stresses on the facesheets were reduced through the dissipation action of STG cores in the simulation under different impact energies. The excellent impact resistant and stress distribution capacity of STG core sandwich panels was demonstrated. In comparison to the simulation results with cylinder support, the equivalent stress in both the front and the back facesheets with plate support was relatively larger. The results were consistent with the contact force results.

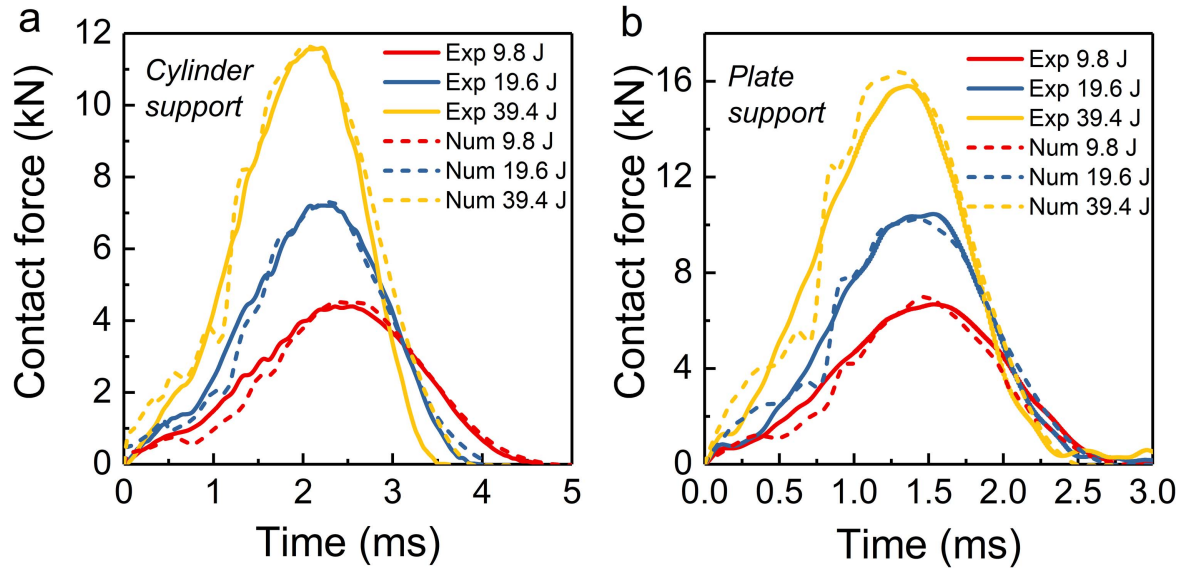

Figure 14. Comparison of numerical and experimental contact force of impact tests with (a) cylinder support and (b) plate support.

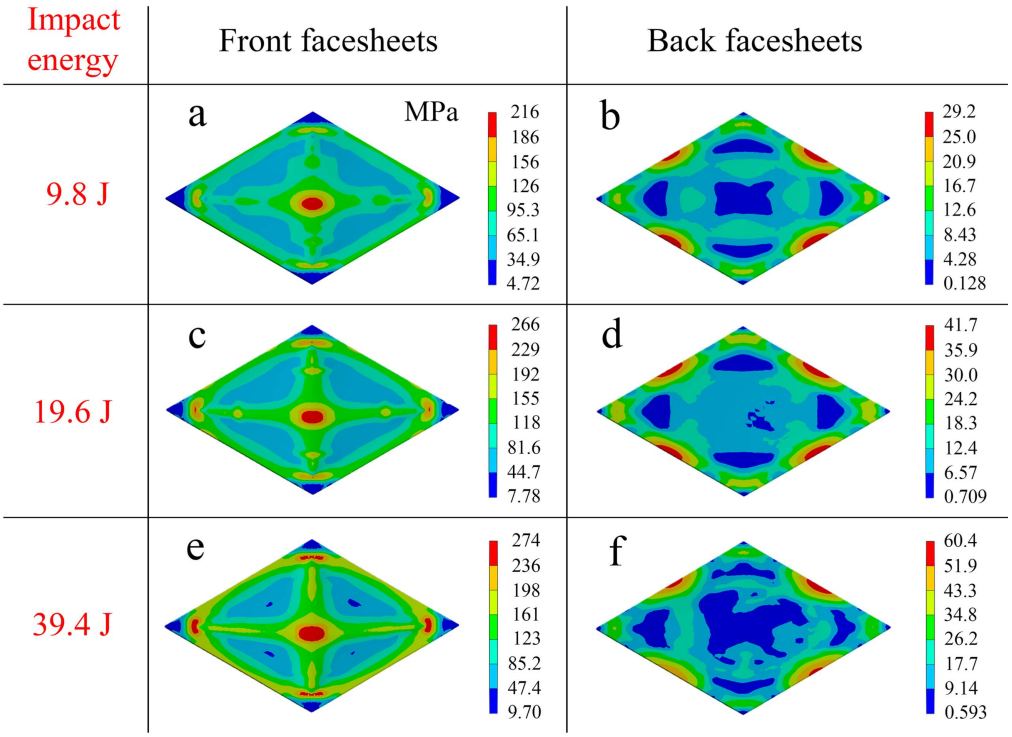

Figure 15. Stress distribution (unit: MPa) in the front facesheets (a), (c), (e) and the back facesheets (b), (d), (f) of STG core sandwich panels in the numerical simulation with cylinder support with impact energy of 9.8 J (a), (b), 19.6 J (c), (d) and 39.4 J (e), (f).

Table 4. The maximum contact force in the experiments and the simulations.

	Cylinder support			Plate support		
Impact energy (J)	9.8	19.6	39.4	9.8	19.6	39.4
Max Exp. force (kN)	4.40	7.21	11.60	6.68	10.46	15.8
Max Num. force (kN)	4.52	7.30	11.65	7.00	10.25	16.40
Error rates (%)	2.7	1.2	0.4	4.8	2.0	3.8

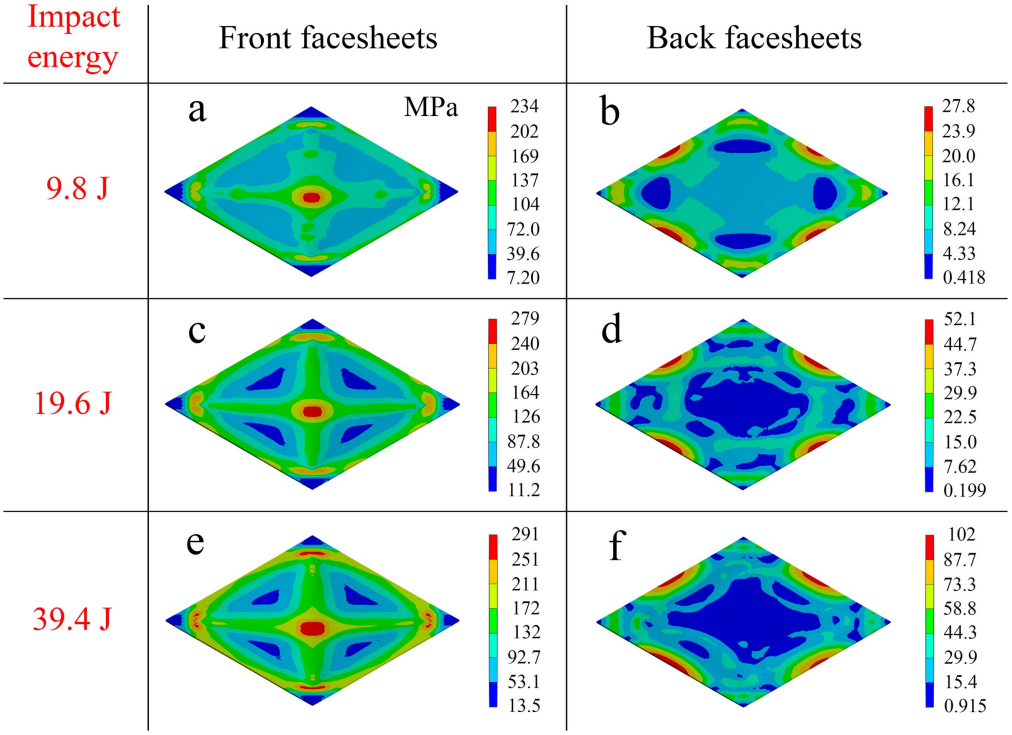

Figure 16. Stress distribution in the front facesheets (a), (c), (e) and back facesheets (b), (d), (f) of Al-STG-Al sandwich panels in the numerical simulation with plate support at the impact energy of 9.8 J (a), (b), 19.6 J (c), (d) and 39.4 J (e), (f).

5. Conclusion

In this work, low-velocity impact responses of sandwich structures with two different facesheets and three different cores were studied. The performances of STG core sandwich panels were compared with the panels with CR cores and EPDM cores. In the impact tests with both cylinder support and plate support, the contact force of Al facesheets sandwich panels with STG cores were obviously smaller than that of sandwich panels with CR cores and EPDM cores, and much more energy was absorbed by the STG core sandwich panel. The flexible sandwich panels with CR facesheets and three different cores were also investigated. Similarly, STG core showed better capacities of energy absorption and stress distribution than CR core and EPDM core. The flexible sandwich panels with CR facesheets showed better properties than Al facesheets sandwich panels, while the former was able to be applied to more complicated working situations.

The finite element analysis numerical simulation of Al-STG-Al sandwich panels was carried out to investigate the stress distribution in the facesheets. Due to the presence of the STG cores, the concentrated stress on the front facesheets were distributed to larger areas on the back facesheets and the peak stresses were reduced greatly. Both the experimental results and the numerical simulation results proved that the sandwich panels with STG cores had much better capacities of energy absorption and stress distribution than the sandwich panels with CR cores and EPDM cores. Based on the above results, it can be concluded that the STG core sandwich structures showed great potential applications in impact resistance and cushioning protection.

Acknowledgments

Financial support from the National Natural Science Foundation of China (Grant No. 11772320, 11372301), the Strategic Priority Research Program of the Chinese Academy of Sciences (Grant No. XDB22040502), and the Fundamental Research Funds for the Central Universities (WK2480000002) is gratefully acknowledged. This study was also supported by the Collaborative Innovation Center of Suzhou Nano Science and Technology.

ORCID iDs

Xinglong Gong https://orcid.org/0000-0001-6997-9526

References

[1] Kolopp A, Rivallant S and Bouvet C 2013 Experimental study of sandwich structures as armour against medium-velocity impacts *Int. J. Impact Eng.* **61** 24–35
[2] Chai G B and Zhu S 2011 A review of low-velocity impact on sandwich structures *Proc. Inst. Mech. Eng.* L **225** 207–30
[3] Liu W, Chen Z, Cheng X, Wang Y, Amankwa A R and Xu J 2016 Design and ballistic penetration of the ceramic composite armor *Composites* B **84** 33–40
[4] Balcı O, Çoban O, Bora M Ö, Akagündüz E and Yalçin E B 2017 Experimental investigation of single and repeated impacts for repaired honeycomb sandwich structures *Mater. Sci. Eng.* A **682** 23–30

[5] Sadeghpour E, Sadighi M and Ohadi A 2016 Free vibration analysis of a debonded curved sandwich beam *Eur. J. Mech.* A **57** 71–84

[6] Sankar A, Natarajan S and Ganapathi M 2016 Dynamic instability analysis of sandwich plates with CNT reinforced facesheets *Compos. Struct.* **146** 187–200

[7] Wang H, Ramakrishnan K R and Shankar K 2016 Experimental study of the medium velocity impact response of sandwich panels with different cores *Mater. Des.* **99** 68–82

[8] Liu D, Liu Y and Sui G 2016 Synthesis and properties of sandwiched films of epoxy resin and graphene/cellulose nanowhiskers paper *Composites* A **84** 87–95

[9] Zhu F, Wang Z, Lu G and Zhao L 2009 Analytical investigation and optimal design of sandwich panels subjected to shock loading *Mater. Des.* **30** 91–100

[10] Singh A K, Davidson B D, Hasseldine B P J and Zehnder A T 2015 Damage resistance of aluminum core honeycomb sandwich panels with carbon/epoxy face sheets *J. Compos. Mater.* **49** 2859–76

[11] Yang S, Qi C, Wang D, Gao R, Hu H and Shu J 2013 A comparative study of ballistic resistance of sandwich panels with aluminum foam and auxetic honeycomb cores *Adv. Mater. Eng.* **5** 589216

[12] Vodenitcharova T, Kabir K and Hoffman M 2012 Indentation of metallic foam core sandwich panels with soft aluminium face sheets *Mater. Sci. Eng.* A **558** 175–85

[13] Xu A, Vodenitcharova T, Kabir K, Flores-Johnson E A and Hoffman M 2014 Finite element analysis of indentation of aluminium foam and sandwich panels with aluminium foam core *Mater. Sci. Eng.* A **599** 125–33

[14] Yaseer Omar M, Xiang C, Gupta N, Strbik O M and Cho K 2015 Syntactic foam core metal matrix sandwich composite: compressive properties and strain rate effects *Mater. Sci. Eng.* A **643** 156–68

[15] Xu M, Huang G, Feng S, Qin X, McShane G J and Stronge W J 2016 Perforation resistance of aluminum/polyethylene sandwich structure *Mater. Des.* **100** 92–101

[16] Choi S B, Park Y K and Cheong C C 1996 Active vibration control of intelligent composite laminate structures incorporating an electro-rheological fluid *J. Intell. Mater. Syst. Struct.* **7** 411–9

[17] Antoine G O and Batra R C 2014 Low speed impact of laminated polymethylmethacrylate/adhesive/polycarbonate plates *Compos. Struct.* **116** 193–210

[18] Avachat S and Zhou M 2015 High-speed digital imaging and computational modeling of hybrid metal-composite plates subjected to water-based impulsive loading *Exp. Mech.* **56** 545–67

[19] Araújo A L, Carvalho V S, Mota Soares C M, Belinha J and Ferreira A J M 2016 Vibration analysis of laminated soft core sandwich plates with piezoelectric sensors and actuators *Compos. Struct.* **151** 91–8

[20] Babu V R and Vasudevan R 2016 Dynamic analysis of tapered laminated composite magnetorheological elastomer (MRE) sandwich plates *Smart Mater. Struct.* **25** 035006

[21] Kozlowska J, Boczkowska A, Czulak A, Przybyszewski B, Holeczek K, Stanik R and Gude M 2016 Novel MRE/CFRP sandwich structures for adaptive vibration control *Smart Mater. Struct.* **25** 035025

[22] Mohammadimehr M and Mostafavifar M 2016 Free vibration analysis of sandwich plate with a transversely flexible core and FG-CNTs reinforced nanocomposite face sheets subjected to magnetic field and temperature-dependent material properties using SGT *Composites* B **94** 253–70

[23] Yildirim T, Ghayesh M H, Li W and Alici G 2016 Experimental nonlinear dynamics of a geometrically imperfect magneto-rheological elastomer sandwich beam *Compos. Struct.* **138** 381–90

[24] Yildirim T, Ghayesh M H, Li W and Alici G 2016 An experimental investigation into nonlinear dynamics of a magneto-rheological elastomer sandwich beam *Smart Mater. Struct.* **25** 015018

[25] Tan Z, Zuo L, Li W, Liu L and Zhai P 2016 Dynamic response of symmetrical and asymmetrical sandwich plates with shear thickening fluid core subjected to penetration loading *Mater. Des.* **94** 105–10

[26] Wei M, Hu G, Jin L, Lin K and Zou D 2016 Forced vibration of a shear thickening fluid sandwich beam *Smart Mater. Struct.* **25** 055041

[27] Tian T, Li W, Ding J, Alici G and Du H 2012 Study of shear-stiffened elastomers *Smart Mater. Struct.* **21** 125009

[28] Cross R 2012 Elastic and viscous properties of Silly Putty *Am. J. Phys.* **80** 870–5

[29] Boland C S, Khan U, Ryan G, Barwich S, Charifou R, Harvey A, Backes C, Li Z, Ferreira M S and Möbius M E 2016 Sensitive electromechanical sensors using viscoelastic graphene-polymer nanocomposites *Science* **354** 1257–60

[30] Golinelli N, Spaggiari A and Dragoni E 2015 Mechanical behaviour of magnetic Silly Putty: viscoelastic and magnetorheological properties *J. Intell. Mater. Syst. Struct.* **28** 953–60

[31] Liang J and Zhang X 2014 Rheological properties of SP in shock transmission application *J. Mater. Civ. Eng.* **27** 04014250

[32] Jiang W, Gong X, Wang S, Chen Q, Zhou H, Jiang W and Xuan S 2014 Strain rate-induced phase transitions in an impact-hardening polymer composite *Appl. Phys. Lett.* **104** 121915

[33] Wang Y, Wang S, Xu C, Xuan S, Jiang W and Gong X 2016 Dynamic behavior of magnetically responsive shear-stiffening gel under high strain rate *Compos. Sci. Technol.* **127** 169–76

[34] Goertz M P, Zhu X Y and Houston J E 2009 Temperature dependent relaxation of a 'solid-liquid' *J. Polym. Sci.* B **47** 1285–90

[35] Wang S, Jiang W, Jiang W, Ye F, Mao Y, Xuan S and Gong X 2014 Multifunctional polymer composite with excellent shear stiffening performance and magnetorheological effect *J. Mater. Chem.* C **2** 7133

[36] Wang S, Xuan S, Jiang W, Jiang W, Yan L, Mao Y, Liu M and Gong X 2015 Rate-dependent and self-healing conductive shear stiffening nanocomposite: a novel safe-guarding material with force sensitivity *J. Mater. Chem.* A **3** 19790–9

[37] O'Masta M R, Compton B G, Gamble E A, Zok F W, Deshpande V S and Wadley H N G 2015 Ballistic impact response of an UHMWPE fiber reinforced laminate encasing of an aluminum-alumina hybrid panel *Int. J. Impact Eng.* **86** 131–44

[38] Ramakrishnan K R, Guérard S, Viot P and Shankar K 2014 Effect of block copolymer nano-reinforcements on the low velocity impact response of sandwich structures *Compos. Struct.* **110** 174–82

[39] Rajaneesh A, Sridhar I and Rajendran S 2014 Relative performance of metal and polymeric foam sandwich plates under low velocity impact *Int. J. Impact Eng.* **65** 126–36

[40] Aydin M and Apalak M K 2016 Experimental damage analysis of Al/SiC functionally graded sandwich plates under ballistic impact *Mater. Sci. Eng.* A **671** 107–17

[41] Wang Z, Tian H, Lu Z and Zhou W 2014 High-speed axial impact of aluminum honeycomb–experiments and simulations *Composites* B **56** 1–8

[42] Wang Z, Lu Z, Yao S, Zhang Y, Hui D and Feo L 2016 Deformation mode evolutional mechanism of honeycomb

structure when undergoing a shallow inclined load *Compos. Struct.* **147** 211–9

[43] Wang S, Xuan S, Wang Y, Xu C, Mao Y, Liu M, Bai L, Jiang W and Gong X 2016 Stretchable polyurethane sponge scaffold strengthened shear stiffening polymer and its enhanced safeguarding performance *ACS Appl. Mater. Interfaces* **8** 4946–54

[44] Buchely M and Maranon A 2015 An engineering model for the penetration of a rigid-rod into a Cowper–Symonds low-strength material *Acta Mech.* **226** 2999–3010

[45] Hernandez C, Maranon A, Ashcroft I and Casas-Rodriguez J 2013 A computational determination of the Cowper–Symonds parameters from a single Taylor test *Appl. Math. Modelling* **37** 4698–708